Running head: SV2-PET imaging in Alzheimer's disease

In vivo imaging of synaptic loss in Alzheimer's disease with [18F]UCB-H Positron Emission Tomography

Christine Bastin, PhD*, Mohamed Ali Bahri, PhD*, François Meyer, MD, Marine Manard, PhD, Emma Delhaye, PhD, Alain Plenevaux, PhD, Guillaume Becker, PhD, Alain Seret, PhD, Christine Mella, QP, Fabrice Giacomelli, PhD, Christian Degueldre, Eng, Evelyne Balteau, PhD, André Luxen, PhD, & Eric Salmon, MD

GIGA-Cyclotron Research Center-in vivo imaging, University of Liège, Allée du 6 Août, B30, 4000 Liege, Belgium

* These authors contributed equally to this work

Corresponding author: Christine Bastin, GIGA-Cyclotron Research Centre-in vivo imaging, University of Liège, Allée du 6 Août, B30, 4000 Liège, Belgium, Telephone: +32 4 366 23 69, Fax: +32 4 366 29 46, Email: Christine.Bastin@uliege.be.

Orcid for the corresponding author: 0000-0002-4556-9490

Abstract

Purpose: Loss of brain synapses is an early pathological feature of Alzheimer's disease. The current study assessed synaptic loss *in vivo* with Positron Emission Tomography and an 18F-labelled radiotracer of the synaptic vesicle protein 2A, [18F]UCB-H.

Methods: Twenty-four patients with Mild Cognitive Impairment or Alzheimer's disease and positive [18F]Flutemetamol amyloid-PET were compared to nineteen healthy controls. [18F]UCB-H brain uptake was quantified with Logan graphical analysis using an image-derived blood input function. SPM12 and regions-of-interest (ROI) analyses were used for group comparisons of regional brain distribution volumes and for correlation with cognitive measures.

Results: A significant decrease of [18F]UCB-H uptake was observed in several cortical areas (11 to 18% difference) and in the thalamus (16% difference), with the largest effect size in the hippocampus (31% difference). Reduced hippocampal uptake was related to patients' cognitive decline (ROI analysis) and unawareness of memory problems (SPM and ROI analyses).

Conclusions: The findings thus highlight predominant synaptic loss in the hippocampus, confirming previous autopsy-based studies and a recent PET study with an 11C-labelled SV2A radiotracer. [18F]UCB-H PET allows to image *in vivo* synaptic changes in Alzheimer's disease and to relate them to patients' cognitive impairment.

Keywords: Alzheimer's disease, biomarker, pathophysiology, PET imaging, synaptic loss.

Introduction

Loss of neurons and synapses constitutes a critical neuropathological feature of Alzheimer's disease (AD), combined with amyloid beta deposits and neurofibrillary tangles. Besides tau pathology, synaptic loss appears as the best correlate of cognitive decline in patients with Mild Cognitive Impairment (MCI) and AD [1, 2].

Post-mortem ultrastructural counts in MCI and AD revealed that the hippocampus and the entorhinal cortex are the most affected by synaptic loss [2-4], followed by the cingulate gyrus and temporal cortex [4]. Basal forebrain is also a site of early neuronal loss in AD, that can precede medial temporal involvement in prodromal AD [5]. Moreover, synaptic dysfunction, indexed by reduced level of expression of pre- and post-synaptic proteins such as synaptophysin or synaptic vesicle protein 2A (SV2A), is observed very early in AD. In MCI, it affects mainly the hippocampus, the temporal cortex [6, 7], and posterior cingulate cortex [8]. In the dementia stage, synaptic dysfunction extends to parietal and frontal areas [6]. Synaptopathy likely heralds the onset of cognitive decline in AD [3]. Given that impaired episodic memory is the initial symptom in the course of typical AD [9] and given the predominance of hippocampal synaptic loss in early AD [3], it is likely that both are related. Memory deficits in AD may also relate to loss of cholinergic neurons in the basal forebrain.

Recently, it has become possible to assess AD-related synaptic loss *in vivo* using PET imaging and tracers with nanomolar affinity for SV2A protein, such as [11C]UCB-J [10], [11C]UCB-A [11], and [18F]UCB-H [12]. SV2A is one of the membrane proteins of synaptic vesicles, contributing to the packaging and transport of neurotransmitters [13]. In AD, autopsy studies showed that the expression of SV2A protein is significantly diminished in the hippocampus and the neocortex [14]. Recently, [11C]UCB-J PET imaging was used to compare cerebral synaptic density between 9 amyloid-positive AD patients (5 MCI and 4

demented patients) and 8 healthy controls [15]. Significant reduction of [11C]UCB-J was found specifically in the hippocampus and entorhinal cortex, with synaptic loss surviving partial volume correction only in the hippocampus. Chen et al. [15] combined patients and controls to observe a correlation between hippocampal synaptic density and a composite episodic memory score. These findings with SV2A-PET imaging open a new avenue for investigating the pathophysiology of AD in vivo [16]. Yet, 11C-labelled radiotracers are ill-suited for broad use, because the short half-life of the carbon-11 prevents transport of the tracer from production sites to remote PET scanning sites. So, a 18F-labelled radiotracer of SV2A protein ($T_{1/2}$ = 110 minutes), like [18F]UCB-H [12], appears as very adequate for a broader use, including clinical practice [16].

Consequently, the aim of the current study was to assess *in vivo* the regional synaptic loss in AD using [18F]UCB-H PET imaging. In previous works, we found that [18F]UCB-H uptake is blocked by pretreatment with levetiracetam in rodents and shows a test-retest variability of 10.4% on the whole brain [12], that there is negligible amount of radiometabolites in the rat brain and that the principal radiometabolite does not cross the blood brain barrier [17], that the radioligand has good biodistribution and dosimetry properties for human PET imaging [18], and that the radiotracer demonstrates the expected homogeneous distribution in the human brain [19]. Concretely, in this study, we compared regional cerebral uptake of [18F]UCB-H between amyloid-positive patients from the AD continuum and healthy older controls. Based on post-mortem findings [2-4] and on the results of the study using [11C]UCB-J PET in AD patients [15], AD patients were expected to demonstrate predominant synaptic loss in the hippocampal structure and also synaptic reduction in the neocortex and the basal forebrain [2, 5, 8]. Correlation between SV2A-PET images and important measures

of cognitive function (i.e., global cognitive decline, memory performance and awareness of everyday cognitive and memory functioning) were also examined.

Material and methods

Participants

Two groups of older participants were included in the study. In the first group, amyloid-positive patients from the AD continuum (Aβ-positive group, n = 25) were recruited from the Memory Clinic at the Liege University Hospital and were diagnosed based on current NIA-AA criteria [9, 20, 21]. As part of the initial diagnostic process, [18F]FDG-PET was used as a biomarker of neurodegeneration in some, but not all patients. Amyloid-β positivity was determined based on [18F]Flutemetamol-PET by qualitative visual inspection and by cortical standardized uptake value ratios (SUVR) above a quantitative threshold determined in a database of healthy older (HO) adults ($SUVR^T$ = SUVR (HO_{mean}) + 2 SUVR (HO_{SD}); cortical SUVR > 1.46). In this group, 6 patients met the criteria for MCI (MMSE between 26 and 30). The remaining 19 Aβ-positive patients were diagnosed with probable AD, with MMSE scores between 14 and 26 (mild stage, MMSE > 20, n = 15; moderate stage, MMSE ≤ 20, n = 4). The second group was composed of cognitively healthy older participants (CTRL, n = 21) (MMSE between 28 and 30). In the control group, amyloid-negativity was confirmed in 8 participants, while there was no biomarker-related information for the others. Both groups were matched in terms of age, sex distribution, and education (Table 1). Mild to moderate white matter lesion was not considered as an exclusion criterion.

Written informed consent was obtained from all participants according to the declaration of Helsinki. The study (EudraCT 2014-000286-50) was approved by the Ethics Committee of the Liege University Hospital.

Neuropsychological assessment

All participants performed a neuropsychological test known to be sensitive to early visual recognition memory deficits related to medial temporal lobe dysfunction (DMS48 [22]). Global cognition was assessed with the MMSE. Everyday life cognitive functioning was assessed by means of informant-based reports and participants' reports with the Anosognosia Questionnaire-Dementia (AQ-D) that probes cognitive and behavioural changes [23], and the Memory Awareness Rating scale-Memory Functioning Scale (MARS-FS) that addresses specifically memory impairment [24]. Inclusion of these scales was motivated by the finding that anosognosia could provide an early cognitive marker of AD [25].

Cerebral image acquisition

Dynamic PET acquisitions were performed using a Siemens/CTI (Knoxville, TN) ECAT HR+ PET scanner. 157.06 ± 8.96 MBq of [18F]UCB-H [26] were injected as an intravenous bolus (injected mass: 0.26 ± 0.21 μg). A thermoplastic mask was used to restrain motion during the acquisition. The timeframe of the dynamic PET was 6x10, 8x30, 5x120, and 17x300 seconds (total = 100 minutes). All PET images were reconstructed using filtered backprojection (Hann filter, 4.9 mm FWHM) including corrections for measured attenuation, dead time, random events, and scatter using standard software (ECAT 7.1, Siemens/CTI, Knoxville, TN). With these acquisition and reconstruction settings, the transaxial resolution in water is 6.5-7 mm in the brain volume (voxel size 2.57 x 2.57 x 2.43 mm^3). Blood samples were collected via a catheter inserted in an arm vein in 13 subjects (7 controls and 6 patients) 3, 5, 15, 45, 60, and 90 min post-injection in order to determine the plasmatic parent fraction with high performance liquid chromatography. A mean unchanged plasma fraction was calculated for

each group and used for modelling [19]. Interestingly, mean unchanged plasma fraction did not differ between groups, $F(1, 11) = 0.06$, $p = 0.80$, and showed relatively little individual variability (coefficient of variation = 10.7 %).

In addition, participants underwent a whole-brain quantitative MRI protocol on a 3T Siemens (Erlangen, Germany) Prisma scanner. Quantitative maps are obtained by combining images using different parameters sensitive to different tissue properties. Multiparameter mapping was based on multi-echo 3D fast low angle shot at 1 mm isotropic resolution [27]. This included three datasets with T1, proton density (PD), and magnetization transfer (MT)–weighted contrasts imposed by the choice of the flip angle (FA = 6° for PD & MT, 21° for T1) and the application of an additional off-resonance Gaussian-shaped RF pulse for the MT-weighted acquisition. One AD patients (mild AD) could not undergo an MRI scan because she had a pacemaker and was excluded from the analysis (final Aβ-positive sample, n = 24).

Data are available from the corresponding author upon request.

Image processing

MRI multiparameter maps were processed with the Voxel-Based Quantification (VBQ) toolbox [27] and SPM12 (Wellcome Trust Centre for Neuroimaging, London, UK) to obtain notably a quantitative MT map as well as segmented images (grey matter, white matter, CSF, “other”), normalized to the standard MNI space using unified segmentation [28]. Modulated grey matter images, resized to 2 mm isotropic voxel size like PET images, were smoothed with an isotropic Gaussian kernel of 8 mm of full-width at half maximum and analysed with voxel-based morphometry to identify atrophied regions in the AD group. Furthermore, spatial normalization parameters were used to normalize the PET images. The

grey matter images across the study sample were used to create a grey matter mask for the statistical analyses.

[18F]UCB-H PET dynamic frames were corrected for motion without reslicing. The PET dynamic images were co-registered to the participant's structural MT image (taking the sum of frames between 2 and 30 min as source image). Then, because of the low resolution of the PET scan and because of our main interest in small structures like the hippocampus and the basal forebrain that are atrophied in early Alzheimer's disease [29], the images were corrected for partial volume effects (PVE) using the "iterative Yang" voxel-wise method implemented in the PETPVC toolbox [30], with grey matter, white matter, CSF and "other" as ROI masks.

The ubiquitous distribution of SV2A in the brain makes very unlikely the identification of a "reference region" (with all its necessary characteristics) [31] for modelling the radiotracer distribution. Yet, in previous studies [15], white matter was taken as reference region to measure binding potential. In our sample, visual inspection of MRI data using the age-related white matter changes visual rating scale [32] by a neurologist blind to group status indicated white matter lesions in 2 controls and 9 patients. Therefore, computation of binding potential using white matter was not appropriate for the current AD population. Moreover, the need of an arterial input function (AIF) is a heavy discomfort for the patient. An alternative method using image-derived input function was shown to be comparable to that using the AIF for [18F]UCB-H PET imaging [19], even if the coefficient of variation for measurements was slightly increased.

So, the input function was derived from dynamic PET images [19]. Briefly, the method extracts time series of radiotracer activity in the carotid arteries [33]. The identification of voxels belonging to the carotids is based on the computation of the Pearson product-

moment correlation coefficient between a “seeding region” and voxels in a mask containing the carotid. As, during the first 2 minutes, radioactivity is mainly localized in the vessels, inducing a large spill-out effect [33], the signal was corrected for this spill-out effect using the geometric transfer matrix approach [34].[1]

For each group, the extracted signal was then corrected using the corresponding mean unchanged plasma fraction to obtain the input function used for modelling. Of note, for individuals with blood samples, we compared the distribution volume estimated using the group mean unchanged plasma fraction (Aβ-positive: 4.24 ± 0.98; control: 4.92 ± 1.02) to the distribution volume estimated using individual unchanged plasma fraction (Aβ-positive: 4.39 ± 1.15; control: 4.76 ± 1.56). Mean whole-brain distribution volume did not significantly differ between the two methods (Aβ-positive: Wilcoxon matched pairs test $Z = 0.31$, $p = 0.75$; control: $Z = 0.98$, $p = 0.32$) and distribution volume across Automated Anatomical Labelling atlas regions strongly correlated between methods ($r = 0.99$ in each group). Kinetic modelling using PVE-corrected dynamic PET data and image derived input function was done with PMOD (Version 3.7, PMOD Technologies, Zurich, Switzerland). Logan graphical analysis was used to calculate the distribution volume (Vt) map of [18F]UCB-H in the brain. The t* for Logan analysis was 25 minutes.

Finally, the Vt map was normalized into the MNI space using transformation parameters obtained during structural MRI spatial normalization (2 mm isotropic voxel size). The PET data of two healthy controls had to be discarded, one because the carotids were not visible on the image and the other because the dynamic acquisition was aborted due to a technical problem (final control sample, n = 19).

Fifteen Aβ-positive patients (4 MCI, 8 mild AD and 3 moderate AD) underwent a [18F]FDG PET scan at the Liege University Hospital less than 4 years before the [18F]UCB-H PET scan

(mean delay between [18F]FDG PET and UCB-H PET scans: 23.8 months ± 12.7; min. 10.3 months, max. 45.5 months). Those PET scans were co-registered to the participant's recent structural MT image, PVE corrected, and normalized into the MNI space using spatial transformation parameters obtained during structural MRI normalization, like [18F]UCB-H PET images.

Statistical analyses

For SPM12 statistical analyses, the normalized PVE-corrected Vt maps were smoothed with an isotropic Gaussian kernel of 8 mm of full-width at half maximum. These Vt maps were entered in a two-sample t-test contrasting images from the Aβ-positive group (n = 24) with those from the control group (n = 19). Parameters were estimated according to the general linear model at each voxel, using a grey matter mask. AD-related regional synaptic loss was tested by a linear contrast (Aβ-positive – controls) with a statistical threshold of $p < 0.05$ with a family-wise (FWE) correction for multiple comparisons at the voxel level (no minimal cluster size). Labelling of significant regions used the Automated Anatomical Labelling atlas, and more specific identification of thalamic nuclei was based on an automated version of Morel's atlas of thalamic nuclei [35]. Furthermore, a sub-analysis comparing only mild AD patients (n = 14) with controls was conducted to examine changes in synaptic density in a group homogeneous in terms of clinical diagnosis criteria and severity. In the Aβ-positive group, SPM12 multiple regression models allowed to test for correlation between regional [18F]UCB-H distribution volume and each cognitive measure (MMSE, DMS48 proportion of correct responses, discrepancy scores between patients' and informants' assessments regarding cognitive and behavioural functioning, indicative of anosognosia) with a statistical threshold of $p < 0.05$ FWE-corrected at the voxel level (no minimal cluster size).

In addition, hypotheses about regional loss of synapses were assessed by comparing the mean Vt values extracted from the unsmoothed normalized PVE-corrected Vt maps of the two groups in 10 regions of interest (ROIs) (averaged across both hemispheres): hippocampus, parahippocampal gyrus, lateral parietal cortex, posterior cingulate cortex, lateral prefrontal cortex, lateral temporal cortex, occipital cortex, thalamus (ROIs built from Automated Anatomical Labelling atlas), and basal forebrain Ch1-3 and Ch4 with stereotaxic probabilistic maps created by microscopic delineations in human postmortem brains [36]. Using Statistica (StatSoft, Inc.), group differences in mean Vt values in the ROIs (considering mainly the whole Aβ-positive group, and also the mild AD subgroup) were assessed with an analysis of variance (ANOVA) with group as between-subject variable and regions as within-subject variable, with an alpha level of 0.05. Post-hoc group comparison for each ROI was computed with Student t tests. Additionally, mean Vt values were extracted from the centrum semiovale and the cerebellum grey matter as “control” regions [15]. For those regions, group differences were tested with Student t test ($p < 0.05$). Effect size of group differences was measured with Cohen’s d corrected for sample size inferior to 50. Pearson correlations between ROI Vt values and cognitive measures were finally computed, considering variability in the Aβ-positive group only. Given the modulating effect of education on cerebral changes, for instance on cholinergic activity [37], Pearson correlations between ROI Vt values and education were also assessed in the Aβ-positive group. Voxel-based morphometry in SPM12 allowed to compare groups in terms of atrophy with a statistical threshold of $p <0.05$ with a FWE correction for multiple comparisons at the voxel level. In the Aβ-positive group, grey matter density was also extracted in the hippocampal ROI and correlated to [18F]UCBH Vt values in the same ROI. Finally, in order to tentatively compare [18F]UCBH measure of synaptic density with [18F]FDG measure of glucose

metabolism in key regions affected by Alzheimer's disease, i.e., the hippocampus and the posterior cingulate cortex, Pearson correlations were used to assess the relationship between [18F]UCBH PVE-corrected Vt values and SUVR taking the pons as reference for [18F]FDG-PET in each ROI in a subgroup of patients (n = 15 with [18F]FDG-PET obtained less than 4 years before [18F]UCBH, including 4 MCI, 8 mild AD and 3 moderate AD patients).

Results

Neuropsychological assessment

The Aβ-positive group demonstrated visual recognition memory impairment (Table 1). Both participants and informants reported more cognitive and behavioural changes, as well as poorer everyday life memory functioning in the Aβ-positive compared to the control group. As a group, Aβ-positive patients were aware of their cognitive difficulties, as suggested by average participant-informant discrepancy scores that did not differ from controls' scores. However, individual variability was large in the patient group, with scores ranging from -0.99 (i.e., overestimation of memory problems) to 1.36 (i.e., underestimation of memory problems) for the MARS-FS.

Imaging measurements

Voxel-wise comparisons of [18F]UCB-H PVE-corrected Vt maps between the Aβ-positive and control groups revealed a significant reduction of synaptic density in the right anterior hippocampus extending to the entorhinal cortex (Figure 1 and Table 2). By comparison to controls' values, Aβ-positive patients demonstrated a 26.9% decrease in right hippocampal [18F]UCB-H distribution volume when considering values from the significant cluster. At a more lenient statistical threshold ($p < 0.10$ FWE-corrected for multiple comparisons, used for

exploratory analyses), there was also reductions in synaptic density in the left hippocampus (27.0% decrease) and in the thalamus (30.2% decrease, with a preferential involvement of the dorsomedial and anterior nuclei of the thalamus) in the Aβ-positive group (Table 2). When considering only mild AD patient (n = 14), the sub-analysis showed reduced synaptic density in the right superior temporal gyrus ($p < 0.05$ FWE-corrected), and, at a more lenient threshold, in the right hippocampus and right middle frontal gyrus ($p < 0.10$ FWE-corrected) (Online Resource 1). SPM12 group comparison using non-PVE corrected images showed less significant difference (the right hippocampus –MNI coordinates 16 -12 -16, k = 12- showed reduced Vt values at an uncorrected threshold of $p < .001$).

In order to further test hypotheses about regions showing synaptic loss in AD, mean Vt values were compared between groups in several ROIs selected according to neuropathological data reported in the introduction. Mean Vt values per ROIs in each group are reported in Table 3, together with the effect size of the group difference and the percentage of uptake reduction in the Aβ-positive group compared to the control group. The ANOVA comparing [18F]UCB-H values as a function of group and ROIs confirmed the significant reduction of synaptic density in Aβ-positive patients [main effect of group, $F(1, 41) = 7.6$, $p < 0.01$] and showed a main effect of regions [$F(9, 369) = 103.6$, $p < 0.001$]. The significant group by region interaction [$F(9, 369) = 2.1$, $p < 0.05$] indicated that Aβ-positive-related synaptic loss is more pronounced in some regions than others. To explore the interaction, follow-up t-tests assessed group differences for each region (Table 3). The largest significant group difference concerned the hippocampus, with a large effect size (Cohen's d = 1.24). All other ROIs, except the basal forebrain Ch4 and the posterior cingulate region, also showed significant group differences. With regard to "control" regions,

[18F]UCB-H values did not differ between groups. The distribution of Vt values in each ROI as a function of group can be seen in Figure 2.

When comparing ROI-based Vt values between mild AD only and healthy controls, we observed significant group differences in the hippocampus (large effect; d = 1.29), parahippocampal cortex, thalamus, parietal and temporal cortex (Online Resource 2). Finally, when Vt values were extracted from non-PVE-corrected PET images, significant reduction of synaptic density in Aβ-positive patients was found in the hippocampus, basal forebrain Ch1-3, parahippocampal cortex and thalamus, with the largest group difference in the basal forebrain Ch1-3 and hippocampus (d = 0.82 and 0.80 respectively, see Online Resource 3). With this radiotracer and with our PET camera, patients' hippocampal uptake values were smaller after PVE correction compared to non-corrected values, whereas values were more stable in other regions, like the parahippocampal region. Although infrequent, such effect of PVE correction has already been described for the hippocampus [38], pointing to a complex spill-over effect in normal and pathological aging.

Voxel-based morphometry analyses comparing grey matter density between groups revealed significant atrophy in the Aβ-positive patients in the hippocampus bilaterally and the left inferior frontal cortex (Table 4). There was a significant correlation between [18F]UCB-H Vt and grey matter density in the hippocampus of Aβ-positive patients (PVE-corrected PET images: $r = 0.78$, $p < 0.001$; non-PVE-corrected images: $r = 0.44$, $p < 0.05$, see Online Resource 4). Moreover, in a subgroup of Aβ-positive patients with [18F]FDG-PET (n = 15), there was no significant correlation between [18F]UCB-H Vt and [18F]FDG SUVR in the hippocampus or the posterior cingulate cortex (hippocampus: $r = 0.30$, $p = 0.29$; posterior cingulate cortex: $r = 0.24$, $p = 0.41$).

Voxel-wise correlations between [18F]UCB-H Vt maps and cognitive measures in SPM12 showed only that variability in the measure of awareness of memory functioning on the MARS-FS was significantly and negatively related to variability in [18F]UCB-H distribution values in the left hippocampus (r = -0.82, peak MNI coordinates: x = -32 y = -34 z = -8, t = 5.25; k = 533; see Figure 3). This correlation indicated that Aβ-positive patients who underestimated their memory problems showed reduced synaptic density in the left hippocampus.

Finally, Pearson correlations were computed between [18F]UCB-H values in the selected ROIs on the one hand and cognitive measures on the other hand (Table 5, Figures 4 and 5 for illustration of significant correlations). MMSE scores correlated with synaptic density in the hippocampus, prefrontal and temporal ROIs. Visual recognition memory (DMS48) was associated with [18F]UCB-H values in the parahippocampal ROI. Degree of unawareness of difficulties (from both the AQ-D and MARS-FS) was related to synaptic density in the hippocampus and posterior cingulate cortex. Additionally, lack of awareness of memory problems (MARS) correlated with synaptic density in the parahippocampal gyrus, thalamus and prefrontal ROIs. Of note, only the correlations between awareness of memory problems and MMSE scores on the one hand and [18F]UCB-H values in the hippocampus on the other hand survived correction for multiple comparisons. With regard to correlation with education, patients with more years of education had higher synaptic density in the parietal area, but this correlation did not hold with correction for multiple comparisons. When using [18F]UCB-H values from non-PVE corrected images, correlations with cognitive scores were mostly similar, although none survived correction for multiple comparisons (DMS48-parahippocampal ROI, r = .47, p = .01; MARS-hippocampal ROI, r = -.45, p = .02; MARS-

posterior cingulate ROI, r = -.49, p = .03; MARS-parahippocampal ROI, r = -.44, p = .03; MARS-thalamus ROI, r = -.42, p = .03), but there was no correlation with the MMSE score anymore.

Discussion

This study reports the topography of synaptic loss *in vivo* in early AD using PET and [18F]UCB-H radiolabelled ligand that binds to SV2A proteins. The main finding is strong evidence of synaptic loss in the hippocampus in amyloid-positive patients from the AD spectrum, with most patients in the early stages of the disease. This result was observed consistently in the whole sample, as well as in mild AD only, with and without PVE correction. SV2A-PET imaging thus allowed to capture the early and prominent hippocampal loss of synapses in AD that was consistently demonstrated in post-mortem analyses [2, 3, 6]. This is also in line with a recent study on SV2A-PET imaging in AD using [11C]UCB-J [15] which demonstrated reduced tracer uptake in the hippocampus.

The hippocampus was significantly atrophied in Aβ-positive patients and [18F]UCB-H uptake and grey matter density correlated in the hippocampus (even more so when PET images were corrected for PVE). Kepe et al. [39] found a similar strong correlation between hippocampal atrophy and serotonin 1A PET data in AD, but showed that PVE had only limited effects on the significant decrease of tracer binding in AD. So, even if the accuracy of PVE-correction for [18F]UCB-H should be assessed, reduced synaptic density after partial volume correction may not merely reflect atrophy. The correlated signal across both measures could stem from a similar cause such as neuronal death [39]. Indeed, although mildly impaired, the Aβ-positive patients were already symptomatic, and so had accumulated substantial neuropathological changes that can be seen through different neuroimaging measures. In order to assess the chronological unfolding of pathological

events, for instance synaptic loss versus atrophy, it would be necessary to perform these measures longitudinally in asymptomatic individuals at high risk of developing AD. Moreover, voxel-wise group comparisons showed additional reduced grey matter density in the prefrontal cortex, whereas additional diminished synaptic density was found in the thalamus. This suggests that [18F]UCB-H measures provide complementary topographical mapping of loss of synapses beyond volume loss.

Derived from [18F]UCB-H uptake, Aβ-positive-related hippocampal reduction in synaptic density was estimated at 26.9% in the right anterior hippocampus when considering the cluster showing significant difference in SPM analyses or at 30.9% when considering the values extracted from the hippocampal ROI. Counts of synapses at autopsy indicated a rate of 44% and 55% of loss in the dentate gyrus and CA1 subfield of the hippocampus respectively in mildly-to-severely demented AD patients compared to healthy older adults [2]. As for MCI patients, they had 13% and 18% fewer synapses in dentate gyrus and CA1 subfield respectively [2]. The rate of 26.9% of reduced hippocampal synaptic density obtained with SV2A-PET imaging plausibly lies between autopsy-based values for MCI and AD patients and likely characterizes early AD stages. It is also very consistent with the 28% reduction in hippocampal Vt reported by Chen et al. [15] with [11C]UCB-J in a small Aβ-positive population.

In addition to the prominent reduction of synaptic density in the hippocampus, ROI-based group comparisons of [18F]UCB-H distribution volume revealed widespread synaptic decline across the neocortex [3, 4] and in some subcortical nuclei in AD patients, including the basal forebrain Ch1-3. Although it is well-established that basal forebrain neurons are very vulnerable to early AD [5], the impact of AD on synapses of this region was never previously reported in vivo. Of note, the reduction of synaptic density was mainly observed in regions

Ch1-3, which contains notably the medial septal nucleus and the diagonal band of Broca, that project to the hippocampal complex [40], but less so in basal forebrain region Ch4, containing nucleus basalis of Meynert and projecting to the amygdala and most cortical regions [36]. Given that loss of cholinergic neurons in AD concerns Ch4 more than Ch1-3 [40], the current findings may rather reflect disconnection of basal forebrain-hippocampal circuit. The voxel-wise analysis also pointed to an important involvement of the thalamus in synaptic loss due to AD. Whereas Chen et al. [15] reported reduced [11C]UCB-J uptake in the pulvinar nucleus, the thalamic areas showing reduced synaptic density in the current Aβ-positive sample are mainly the dorsomedial nucleus and anterior nucleus. These nuclei are connected to the entorhinal cortex and hippocampus respectively [41], as well as to the prefrontal cortex [42]. Thus, the findings of reduced [18F]UCB-H distribution volume in the hippocampus, basal forebrain, and anterior/dorsomedial thalamus suggests a particular vulnerability of medial temporal-frontal lobe circuits to early synaptic loss in the course of AD.

In the current design, [18F]FDG-PET was used as a biomarker of neurodegeneration to increase our probability of AD diagnosis in some patients. At visual inspection, a typical pattern of hypometabolism in the temporoparietal areas and posterior cingulate cortex was observed. Interestingly, in 15 Aβ-positive patients who underwent the [18F]FDG-PET scan less than 4 years before the current study, no relationship was found between reduction of synaptic density and hypometabolism in the hippocampus and in the posterior cingulate cortex. Although this could indicate a chronological effect of the pathology due to the delay between the two PET explorations, this might also suggest that the two radiotracers measure different pathological mechanisms. Future studies using [18F]UCB-H and [18F]FDG

PET imaging acquired at the same time period could inform about metabolic changes in brain networks that correlate to hippocampal synaptic loss.

Consistently with autopsy studies that related synaptic loss to cognitive impairment [3, 8], global cognitive decline, as assessed by the MMSE, correlated with [18F]UCB-H uptake values in the hippocampus measured with ROI. If progression of synaptic loss follows the same pattern as neurofibrillary tangles, with initial pathology in the medial temporal lobe, this correlation would indicate that cognitive decline in our group of mostly mildly impaired patients is associated with early sites of synaptic loss and neuronal death. In addition, ROI-based analyses indicated that visual recognition memory performance on DMS48 correlated with synaptic density in the parahippocampal gyrus (although not surviving correction for multiple comparisons). This finding suggests that PET imaging of SV2A protein allows a precise and specific mapping of behaviour and synaptic changes. Indeed, the DMS48 has been previously shown to be sensitive to dysfunction of the entorhinal and perirhinal cortices [22].

Interestingly, there was a significant correlation between the degree of awareness of memory problems in patients and synaptic density in the hippocampus (surviving correction for multiple comparisons in both the voxel-wise and ROI-based analyses), posterior cingulate cortex, parahippocampal cortex, thalamus, and prefrontal cortex. The measure of anosognosia for memory problems varied largely in the current sample. The current finding suggests that patients who were less aware of their memory difficulties had reduced synaptic density in the hippocampus, as well as in connected regions. This circuit, critical for episodic memory [41], would be important to remember everyday life instances of forgetfulness, so as to update knowledge about one's current memory status [43]. The correlation with the posterior cingulate cortex synaptic density is consistent with its

integrative function by which the outcomes of retrieved self-knowledge and inference mechanisms are combined to reflect about one's own current memory abilities [44]. Again, the fact that different regions show a correlation between their [18F]UCB-H uptake values and distinct cognitive tasks suggest that SV2A-PET imaging could be a sensitive tool to localize relationships between synaptic loss and cognitive decline in a domain-specific manner.

One limitation of the current study is the fact that only 8 control participants had a [18F]Flutemetamol PET scan to confirm the absence of amyloid deposit in their brain. This leaves open the possibility that some of the other control participants were actually amyloid positive. Despite the fact that this may have reduced the power to detect differences, it is noticeable that the Aβ-positive group was found to have reduced [18F]UCB-H uptake in the hippocampus in voxel-wise SPM analysis with the strictest statistical threshold. Another limitation is the delay separating [18F]FDG-PET and SV2A-PET imaging, but this comparison in a subgroup of patients was not the main goal of the current study. From a methodological viewpoint, the study confirms the possibility and the interest to use an image-based blood input function for the modelisation of [18F]UCB-H brain distribution. Moreover, a validation of the most appropriate method for PVE correction still needs to be done for [18F]UCB-H, notably to assess whether the decrease of Vt values in the hippocampus and the stronger correlation with hippocampal atrophy after PVE correction reflect genuine results or are related to the correction method. Also, the use of the carotid image-derived input function should be validated in a larger sample including AD patients. Finally, we should emphasize that [18F]UCB-H provides a measurement of synaptic *vesicle* density that we use as a proxy to assess decreased synaptic density.

Altogether, the current study demonstrates that SV2A-PET imaging, here with [18F]UCB-H, allows to image *in vivo* synaptic changes in Aβ-positive patients and to relate them to cognitive impairment with regional specificity according to the cognitive domain. These findings confirm and extend those obtained with [11C]UCB-J. So, SV2A-PET imaging represents a new reliable tool to assess critical neuropathological changes during the lifetime of a patient, and the long-lived 18F-labelled tracer would allow its use in widespread research and clinical settings [16]. Moreover, it would provide a unique way to study synaptic loss in other dementias, like frontotemporal lobar degeneration. Finally, given that synaptic dysfunction precedes synapse loss and neuronal death in the cascade of pathogenic molecular changes leading to AD, novel therapeutic strategies may target reversible synaptic dysfunction and the benefit of such treatments would be ideally monitored by SV2A-PET scanning.

Footnotes

1. Signal from the two carotids was used to increase the quality of the data, but distribution volumes obtained by considering the signal from the left and right carotid independently were highly similar (left/right ratio=0.99 ± 0.05) and each was also highly similar to the distribution volume considering the two carotids together (left/total ratio: 0.99 ± 0.01; right/total ratio: 0.99 ± 0.04).

Acknowledgements

This work was supported by grants from Belgian Interuniversity Attraction Pole (IUAP 7/11), ULiege Research Concerted Action (ARC 12/17-01), Special Research Funds classical grant 2016 (Faculty of Medicine, University of Liege, Belgium), FRS-FNRS. Patient selection was supported by an Investigator Sponsored Study (ISS290) from GE Healthcare for [18F]flutemetamol delivery, and the Walloon Region Public Private Partnership NeuroCom, with the ULiege and UCB Pharma as partners. A. Plenevaux is a research director and C. Bastin is a research associate at the FRS-FNRS Belgium. We thank Nicolas Antoine for providing [18F]flutemetamol data, Lola Danet for help with localization of thalamic nuclei in Morel's atlas and Roland Hustinx and Claire Bernard (Liege University Hospital) for providing [18F]FDG-PET images.

Compliance with Ethical Standards

The authors declare that they have no conflict of interest.

Ethical approval

All procedures performed in studies involving human participants were in accordance with the ethical standards of the institutional research committee (Ethics Committee of the Liege University Hospital, reference number EudraCT 2014-000286-50) and with the 1964 Helsinki declaration and its later amendments or comparable ethical standards.

References

1. Terry RD, Masliah E, Salmon DP, Butters N, DeTeresa R, Hill R, et al. Physical basis of cognitive alterations in Alzheimer's disease: synapse loss is the major correlate of cognitive impairment. Ann Neurol. 1991;30:572-80. doi:10.1002/ana.410300410.

2. Scheff SW, Price DA, Schmitt FA, Mufson EJ. Hippocampal synaptic loss in early Alzheimer's disease and mild cognitive impairment. Neurobiol Aging. 2006;27:1372-84. doi:10.1016/j.neurobiolaging.2005.09.012.

3. Honer W. Pathology of presynaptic proteins in Alzheimer's disease: more than simple loss of terminals. Neurobiol Aging. 2003;24:1047-62. doi:10.1016/j.neurobiolaging.2003.04.005.

4. de Wilde MC, Overk CR, Sijben JW, Masliah E. Meta-analysis of synaptic pathology in Alzheimer's disease reveals selective molecular vesicular machinery vulnerability. Alzheimers Dement. 2016;12:633-44. doi:10.1016/j.jalz.2015.12.005.

5. Schmitz TW, Nathan Spreng R, Alzheimer's Disease Neuroimaging I. Basal forebrain degeneration precedes and predicts the cortical spread of Alzheimer's pathology. Nat Commun. 2016;7:13249. doi:10.1038/ncomms13249.

6. Counts SE, Nadeem M, Lad SP, Wuu J, Mufson EJ. Differential expression of synaptic proteins in the frontal and temporal cortex of elderly subjects with mild cognitive impairment. J Neuropathol Exp Neurol. 2006;65:592-601.

7. Counts SE, He B, Nadeem M, Wuu J, Scheff SW, Mufson EJ. Hippocampal drebrin loss in mild cognitive impairment. Neurodegener Dis. 2012;10:216-9. doi:10.1159/000333122.

8. Scheff SW, Price DA, Ansari MA, Roberts KN, Schmitt FA, Ikonomovic MD, et al. Synaptic change in the posterior cingulate gyrus in the progression of Alzheimer's disease. J Alzheimers Dis. 2015;43:1073-90. doi:10.3233/JAD-141518.

9. McKhann GM, Knopman DS, Chertkow H, Hyman BT, Jack CR, Jr., Kawas CH, et al. The diagnosis of dementia due to Alzheimer's disease: recommendations from the National Institute on

Aging-Alzheimer's Association workgroups on diagnostic guidelines for Alzheimer's disease. Alzheimers Dement. 2011;7:263-9. doi:10.1016/j.jalz.2011.03.005.

10. Nabulsi NB, Mercier J, Holden D, Carre S, Najafzadeh S, Vandergeten MC, et al. Synthesis and Preclinical Evaluation of 11C-UCB-J as a PET Tracer for Imaging the Synaptic Vesicle Glycoprotein 2A in the Brain. J Nucl Med. 2016;57:777-84. doi:10.2967/jnumed.115.168179.

11. Estrada S, Lubberink M, Thibblin A, Sprycha M, Buchanan T, Mestdagh N, et al. [(11)C]UCB-A, a novel PET tracer for synaptic vesicle protein 2A. Nucl Med Biol. 2016;43:325-32. doi:10.1016/j.nucmedbio.2016.03.004.

12. Warnock GI, Aerts J, Bahri MA, Bretin F, Lemaire C, Giacomelli F, et al. Evaluation of 18F-UCB-H as a novel PET tracer for synaptic vesicle protein 2A in the brain. J Nucl Med. 2014;55:1336-41. doi:10.2967/jnumed.113.136143.

13. Elferink LA, Scheller RH. Synaptic vesicle proteins and regulated exocytosis. Prog Brain Res. 1995;105:79-85.

14. Robinson JL, Molina-Porcel L, Corrada MM, Raible K, Lee EB, Lee VM, et al. Perforant path synaptic loss correlates with cognitive impairment and Alzheimer's disease in the oldest-old. Brain. 2014;137:2578-87. doi:10.1093/brain/awu190.

15. Chen M, Mecca AP, Naganawa M, et al. Assessing synaptic density in alzheimer disease with synaptic vesicle glycoprotein 2a positron emission tomographic imaging. JAMA Neurology. 2018. doi:10.1001/jamaneurol.2018.1836.

16. Mormino EC, Jagust WJ. A new tool for clinical neuroscience—synaptic imaging. JAMA Neurology. 2018. doi:10.1001/jamaneurol.2018.1643.

17. Becker G, Warnier C, Serrano ME, Bahri MA, Mercier J, Lemaire C, et al. Pharmacokinetic Characterization of [(18)F]UCB-H PET Radiopharmaceutical in the Rat Brain. Mol Pharm. 2017;14:2719-25. doi:10.1021/acs.molpharmaceut.7b00235.

18. Bretin F, Bahri MA, Bernard C, Warnock G, Aerts J, Mestdagh N, et al. Biodistribution and Radiation Dosimetry for the Novel SV2A Radiotracer [(18)F]UCB-H: First-in-Human Study. Mol Imaging Biol. 2015;17:557-64. doi:10.1007/s11307-014-0820-6.

19. Bahri MA, Plenevaux A, Aerts J, Bastin C, Becker G, Mercier J, et al. Measuring brain synaptic vesicle protein 2A with positron emission tomography and [(18)F]UCB-H. Alzheimers Dement (N Y). 2017;3:481-6. doi:10.1016/j.trci.2017.08.004.

20. Albert MS, DeKosky ST, Dickson D, Dubois B, Feldman HH, Fox NC, et al. The diagnosis of mild cognitive impairment due to Alzheimer's disease: recommendations from the National Institute on Aging-Alzheimer's Association workgroups on diagnostic guidelines for Alzheimer's disease. Alzheimers Dement. 2011;7:270-9. doi:10.1016/j.jalz.2011.03.008.

21. Jack CR, Jr., Bennett DA, Blennow K, Carrillo MC, Dunn B, Haeberlein SB, et al. NIA-AA Research Framework: Toward a biological definition of Alzheimer's disease. Alzheimers Dement. 2018;14:535-62. doi:10.1016/j.jalz.2018.02.018.

22. Didic M, Ranjeva JP, Barbeau E, Confort-Gouny S, Fur YL, Felician O, et al. Impaired visual recognition memory in amnestic mild cognitive impairment is associated with mesiotemporal metabolic changes on magnetic resonance spectroscopic imaging. J Alzheimers Dis. 2010;22:1269-79. doi:10.3233/JAD-2010-101257.

23. Migliorelli R, Teson A, Sabe L, Petracca G, Petracchi M, Leiguarda R, et al. Anosognosia in Alzheimer's disease: A study of associated factors. The Journal of Neuropsychiatry and Clinical Neurosciences. 1995;7:338-44.

24. Clare L, Wilson BA, Carter G, Roth I, Hodges JR. Assessing awareness in early-stage Alzheimer's disease: development and piloting of the Memory Awareness Rating Scale. Neuropsychol Rehabil. 2002;12:341-62.

25. Cacciamani F, Tandetnik C, Gagliardi G, Bertin H, Habert MO, Hampel H, et al. Low Cognitive Awareness, but Not Complaint, is a Good Marker of Preclinical Alzheimer's Disease. J Alzheimers Dis. 2017;59:753-62. doi:10.3233/JAD-170399.

26. Warnier C, Lemaire C, Becker G, Zaragoza G, Giacomelli F, Aerts J, et al. Enabling Efficient Positron Emission Tomography (PET) Imaging of Synaptic Vesicle Glycoprotein 2A (SV2A) with a Robust and One-Step Radiosynthesis of a Highly Potent 18F-Labeled Ligand ([18F]UCB-H). J Med Chem. 2016;59:8955-66. doi:10.1021/acs.jmedchem.6b00905.

27. Draganski B, Ashburner J, Hutton C, Kherif F, Frackowiak RS, Helms G, et al. Regional specificity of MRI contrast parameter changes in normal ageing revealed by voxel-based quantification (VBQ). Neuroimage. 2011;55:1423-34. doi:10.1016/j.neuroimage.2011.01.052.

28. Ashburner J, Friston KJ. Unified segmentation. Neuroimage. 2005;26:839-51. doi:10.1016/j.neuroimage.2005.02.018.

29. Erlandsson K, Buvat I, Pretorius PH, Thomas BA, Hutton BF. A review of partial volume correction techniques for emission tomography and their applications in neurology, cardiology and oncology. Phys Med Biol. 2012;57:R119-R59. doi:10.1088/0031-9155/57/21/r119.

30. Thomas BA, Cuplov V, Bousse A, Mendes A, Thielemans K, Hutton BF, et al. PETPVC: a toolbox for performing partial volume correction techniques in positron emission tomography. Phys Med Biol. 2016;61:7975-93. doi:10.1088/0031-9155/61/22/7975.

31. Salinas CA, Searle GE, Gunn RN. The simplified reference tissue model: model assumption violations and their impact on binding potential. J Cereb Blood Flow Metab. 2015;35:304-11. doi:10.1038/jcbfm.2014.202.

32. Wahlund LO, Barkhof F, Fazekas F, Bronge L, Augustin M, Sjogren M, et al. A new rating scale for age-related white matter changes applicable to MRI and CT. Stroke. 2001;32:1318-22.

33. Schain M, Benjaminsson S, Varnäs K, Forsberg A, Halldin C, Lansner A, et al. Arterial Input Function Derived from Pairwise Correlations Between PET-image Voxels. J Cereb Blood Flow Metab. 2013;33:1058-65. doi:10.1038/jcbfm.2013.47.

34. Rousset OG, Ma Y, Evans AC. Correction for partial volume effects in PET: principle and validation. J Nucl Med. 1998;39:904-11.

35. Krauth A, Blanc R, Poveda A, Jeanmonod D, Morel A, Székely G. A mean three-dimensional atlas of the human thalamus: Generation from multiple histological data. Neuroimage. 2010;49:2053-62. doi:https://doi.org/10.1016/j.neuroimage.2009.10.042.

36. Zaborszky L, Hoemke L, Mohlberg H, Schleicher A, Amunts K, Zilles K. Stereotaxic probabilistic maps of the magnocellular cell groups in human basal forebrain. Neuroimage. 2008;42:1127-41. doi:10.1016/j.neuroimage.2008.05.055.

37. Garibotto V, Tettamanti M, Marcone A, Florea I, Panzacchi A, Moresco R, et al. Cholinergic activity correlates with reserve proxies in Alzheimer's disease. Neurobiol Aging. 2013;34:2694 e13-8. doi:10.1016/j.neurobiolaging.2013.05.020.

38. Thomas BA, Erlandsson K, Modat M, Thurfjell L, Vandenberghe R, Ourselin S, et al. The importance of appropriate partial volume correction for PET quantification in Alzheimer's disease. Eur J Nucl Med Mol Imaging. 2011;38:1104-19. doi:10.1007/s00259-011-1745-9.

39. Kepe V, Barrio JR, Huang SC, Ercoli L, Siddarth P, Shoghi-Jadid K, et al. Serotonin 1A receptors in the living brain of Alzheimer's disease patients. Proc Natl Acad Sci U S A. 2006;103:702-7. doi:10.1073/pnas.0510237103.

40. Liu AK, Chang RC, Pearce RK, Gentleman SM. Nucleus basalis of Meynert revisited: anatomy, history and differential involvement in Alzheimer's and Parkinson's disease. Acta Neuropathol. 2015;129:527-40. doi:10.1007/s00401-015-1392-5.

41. Aggleton JP. Multiple anatomical systems embedded within the primate medial temporal lobe: implications for hippocampal function. Neurosci Biobehav Rev. 2012;36:1579-96. doi:10.1016/j.neubiorev.2011.09.005.

42. Johansen-Berg H, Behrens TE, Sillery E, Ciccarelli O, Thompson AJ, Smith SM, et al. Functional-anatomical validation and individual variation of diffusion tractography-based segmentation of the human thalamus. Cereb Cortex. 2005;15:31-9. doi:10.1093/cercor/bhh105.

43. Morris RG, Mograbi DC. Anosognosia, autobiographical memory and self knowledge in Alzheimer's disease. Cortex. 2013;49:1553-65.

44. Leech R, Sharp DJ. The role of the posterior cingulate cortex in cognition and disease. Brain. 2014;137:12-32. doi:10.1093/brain/awt162.

Figure legends

Fig 1 SPM12 results of between-group comparison with [18F]UCB-H distribution volumes: Regions showing reduced synaptic density in amyloid-positive patients compared to healthy controls. Hippocampal cluster rendered on a canonical T1 image ($p < 0.05$ FWE-corrected)

Fig 2 Plots showing [18F]UCB-H Vt values for each region of interest as a function of group (controls, MCI, mild and moderate amyloid-positive patients). Each dot represents a subject's Vt value

Fig 3 SPM12 results of correlation with [18F]UCB-H distribution volumes: the hippocampus showing smaller synaptic density correlated with poorer awareness of memory functioning in Aβ-positive individuals ($p < 0.05$ FWE-corrected)

Fig 4 Scatter plots of significant correlations between [18F]UCB-H distribution values (from images corrected for partial volume effect) in regions of interest (ROI) and MMSE (Mini Mental State Examination) and AQ-D (Anosognosia Questionnaire-Dementia discrepancy score) in the Aβ-positive patients group. * $p < .05$; ** $p < .01$; *** $p < .005$

Fig 5 Scatter plots of significant correlations between [18F]UCB-H distribution values (from images corrected for partial volume effect) in regions of interest (ROI) and MARS-FS (Memory Awareness Rating Scale-Functioning Scale discrepancy score) and DMS48 (visual recognition memory) in the Aβ-positive patients group. * $p < .05$; *** $p < .005$

Figure 1

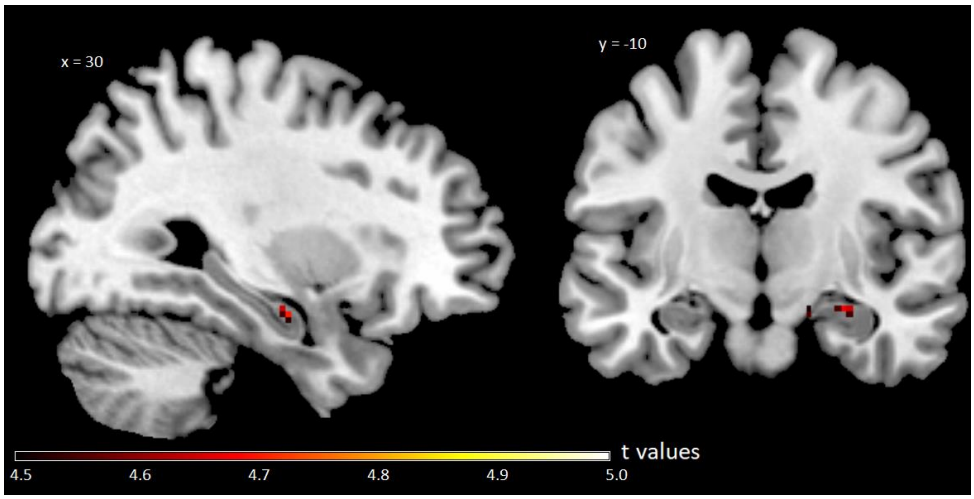

Figure 2

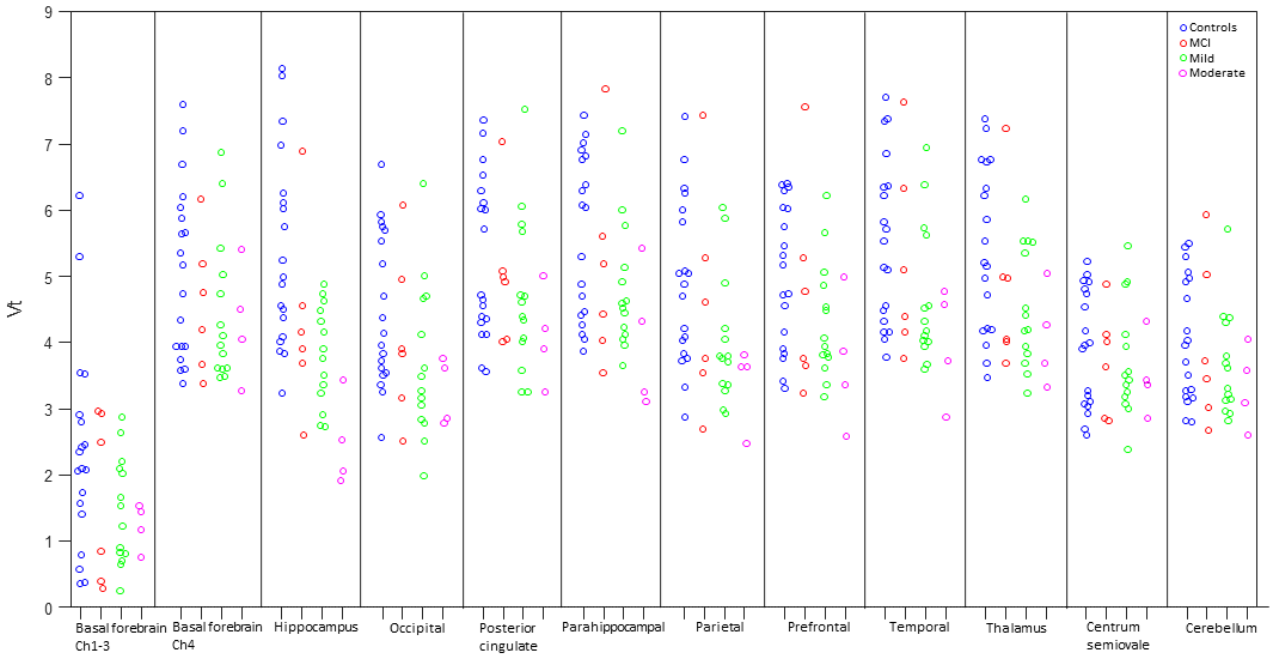

Figure 3

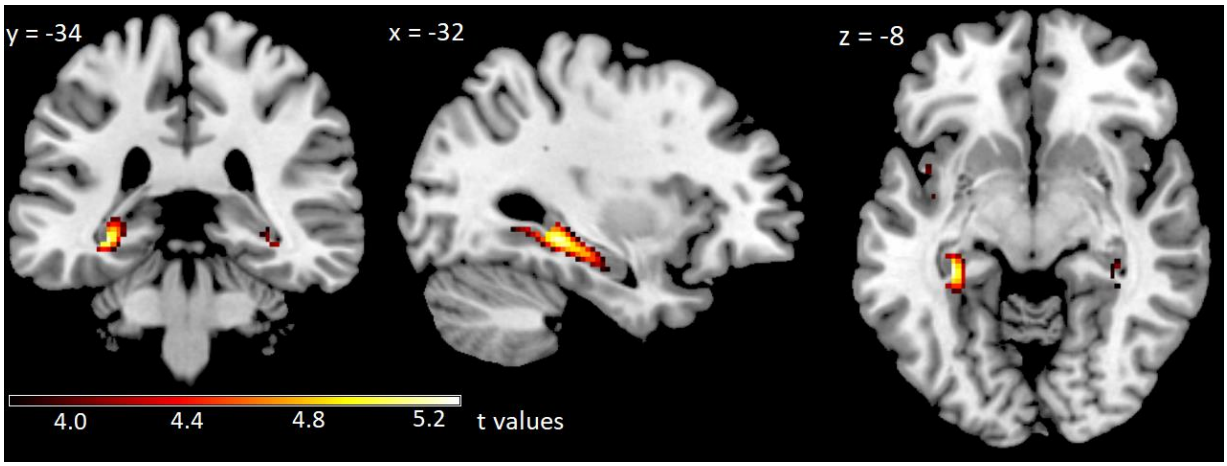

Figure 4

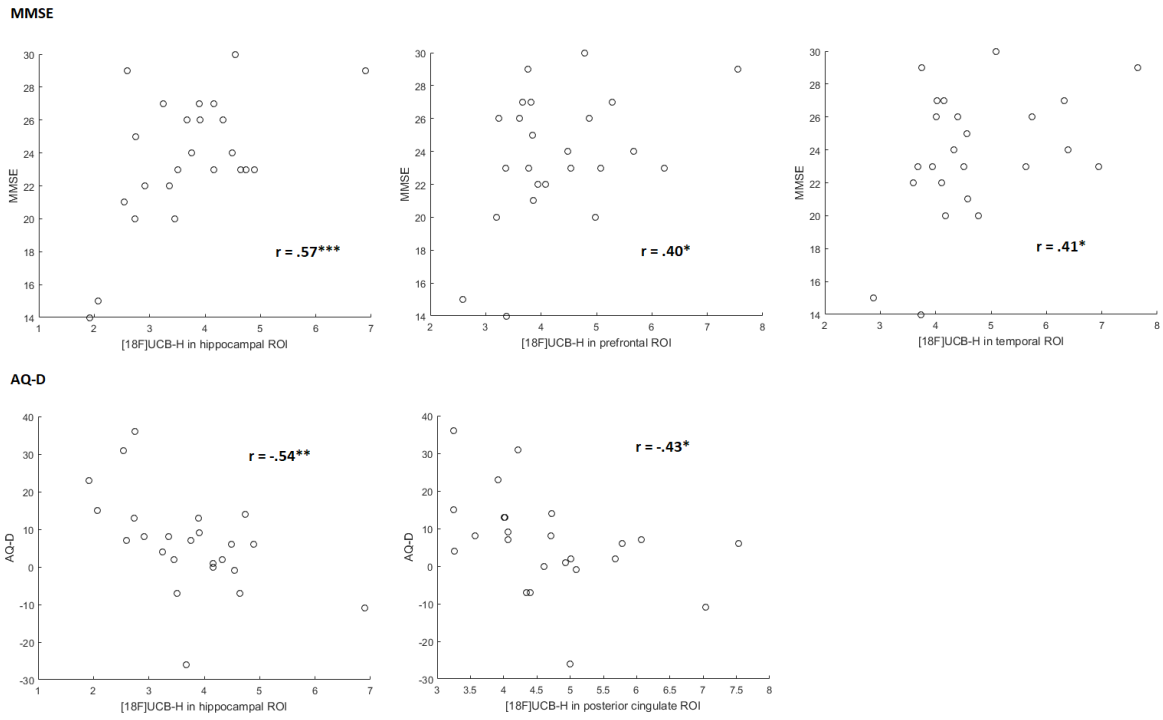

Figure 5

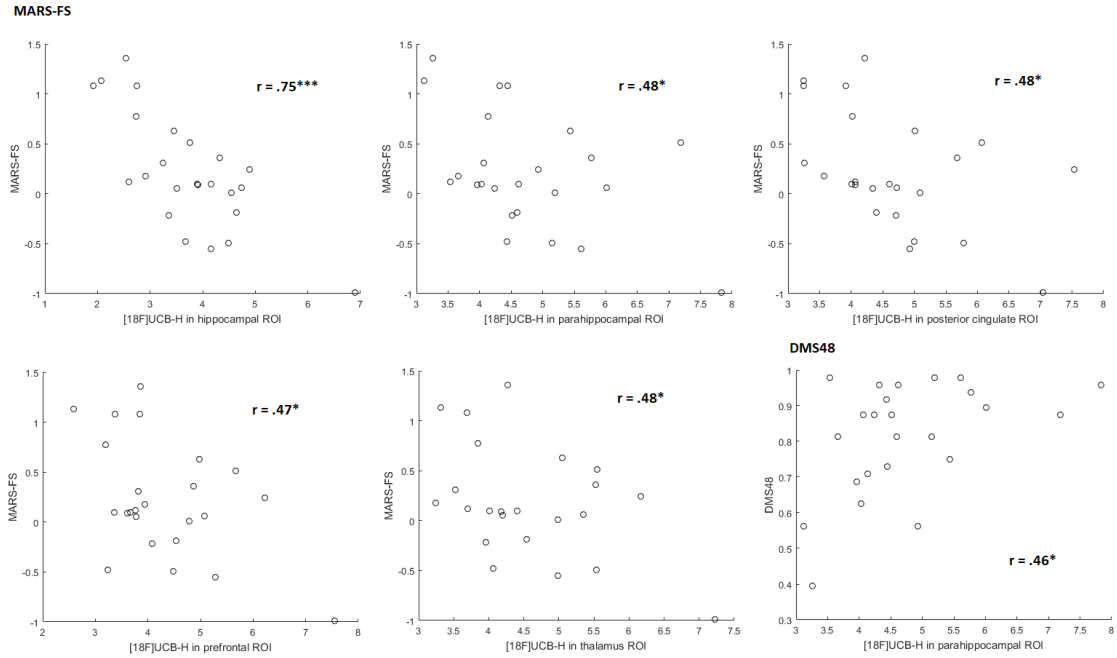
MARS-FS
r = .75***
MARS-FS
[18F]UCB-H in hippocampal ROI
r = .48*
MARS-FS
[18F]UCB-H in parahippocampal ROI
r = .48*
MARS-FS
[18F]UCB-H in posterior cingulate ROI
r = .47*
MARS-FS
[18F]UCB-H in prefrontal ROI
r = .48*
MARS-FS
[18F]UCB-H in thalamus ROI
DMS48
r = .46*
DMS48
[18F]UCB-H in parahippocampal ROI

Table 1. Demographics, clinical characteristics and neuropsychological scores of patient and control groups.

	Aβ-positive patients (n = 25)	Controls (n = 21)	
Age	73.3 (8.0)	71.5 (4.5)	t(44) = -0.9, p = 0.37
Women/men	14/11	10/11	Chi^2 = 0.32, p = 0.57
Education (years)	12.8 (3.6)	13.0 (3.4)	t(44) = 0.1, p = 0.87
MMSE	23.7 (3.9)	29.2 (1.1)	t(44) = 6.3, p < 0.001
DMS48-% correct	.81 (.15)	.98 (.02)	t(42) = 4.8, p < 0.001
AQ-D			
Auto-assessment	19.7 (9.6)	8.4 (5.5)	t(42)= -4.5, p < 0.001
Hetero-assessment	25.6 (10.7)	9.5 (6.7)	t(41) = -5.6, p < 0.001
Discrepancy score	5.8 (12.9)	1.3 (6.4)	t(41) = -1.4, p = 0.17
MARS-FS			
Auto-assessment	33.3 (8.1)	43.7 (4.5)	t(42) = 5.0, p < 0.001
Hetero-assessment	27.8 (8.9)	43.1 (5.5)	t(41) = 6.4, p < 0.001
Discrepancy score	0.21 (0.57)	0.03 (0.15)	t(41) = -1.3, p = 0.19

Note: Standard deviations in parentheses. Aβ, amyloid beta; MMSE, Mini Mental State Examination; DMS48, visual recognition memory; AQ-D, Anosognosia Questionnaire-Dementia [higher scores in auto- and hetero-assessment indicate increased difficulties]; MARS-FS, Memory Awareness Rating scale-Memory Functioning Scale [higher scores in auto- and hetero-assessment indicate good memory functioning].

Table 2. SPM12 analysis of [18F]UCB-H PVE-corrected Vt maps: Peak MNI coordinates of brain regions showing significant reduction in synaptic density in Aβ-positive patients patients compared to controls

Regions	Cluster size	*x*	*y*	*z*	*Z* score
Right anterior hippocampus**	358	14	-8	-18	4.22
		30	-10	-18	4.18
Left hippocampus*	434	-30	-12	-16	3.99
Thalamus*	72	6	-4	8	3.95

* p <0.10 FWE-corrected at the voxel-level; ** p <0.05 FWE-corrected at the voxel-level. PVE, partial volume effect; Vt, distribution volume; MNI, Montreal Neurological Institute; Aβ, amyloid beta; FWE, family-wise error.

Table 3. [18F]UCB-H mean values from PVE-corrected Vt maps in ROIs as a function of group

ROI	Aβ-positive patients	Controls		% diff	Effect size (d)
Hippocampus	3.7 (1.0)	5.4 (1.4)	t(41)=4.2, p<0.001	-30.9	1.24
Basal forebrain Ch1-3	1.5 (0.9)	2.3 (1.5)	t(41)=2.3, p<0.05	-37.3	0.67
Basal forebrain Ch4	4.5 (1.0)	5.1 (1.3)	t(41)=1.7, p=0.08	-12.3	0.51
Parahippocampal	4.7 (1.1)	5.6 (1.2)	t(41)=2.4, p<0.05	-15.6	0.71
Thalamus	4.5 (0.9)	5.4 (1.2)	t(41)=2.5, p<0.05	-15.9	0.73
Parietal	4.0 (1.1)	4.9 (1.2)	t(41)=2.3, p<0.05	-17.6	0.69
Posterior cingulate	4.7 (1.1)	5.3 (1.2)	t(41)=1.6, p=0.10	-11.3	0.49
Prefrontal	4.3 (1.1)	5.0 (1.1)	t(41)=2.0, p<0.05	-14.3	0.63
Temporal	4.7 (1.2)	5.5 (1.2)	t(41)=2.2, p<0.05	-14.9	0.65
Occipital	3.7 (1.1)	4.5 (1.1)	t(41)=2.2, p<0.05	-17.2	0.65
"Control" regions					
Centrum semiovale	3.7 (0.8)	3.9 (0.9)	t(41)=0.8, p=0.38	-5.7	0.25
Cerebellum	3.7 (0.9)	4.0 (0.9)	t(41)=1.2, p=0.21	-8.7	0.37

Note: Standard deviations in parentheses. ROI, region of interest. % diff = (mean Aβ-positive patients – mean controls)/mean controls x 100%. PVE, partial volume effect; Vt, distribution volume; Aβ, amyloid beta; ROI, region of interest. d: Cohen's d for effect size corrected for sample size inferior to 50.

Table 4. SPM12 analysis of grey matter density: Peak MNI coordinates of brain regions showing significant atrophy in Aβ-positive patients patients compared to controls ($p < 0.05$ FWE-corrected at the voxel-level)

Regions	Cluster size	*x*	*y*	*z*	*Z* score
Right hippocampus	2395	20	-6	-12	5.59
		28	-10	-16	5.16
Left hippocampus	3618	-38	-22	-14	4.97
		-30	-10	-16	4.83
		-38	-14	12	4.87
Left inferior frontal cortex	434	-66	-22	32	4.81

Notes. MNI, Montreal Neurological Institute; Aβ, amyloid beta; FWE, family-wise error.

Table 5. Correlation coefficients for Pearson correlations between [18F]UCB-H distribution values (from PVE-corrected images) in selected ROIs and cognitive scores and education in the Aβ-positive patients group

	MMSE	AQ-D	MARS-FS	DMS48	Education
Hippocampus	0.57***	-0.54**	-0.75***	0.29	.32
Parahippocampal	0.34	-0.34	-0.48*	0.46*	.38
Parietal	0.37	-0.24	-0.36	0.14	.41*
Posterior cingulate	0.28	-0.43*	-0.48*	0.14	.23
Prefrontal	0.40*	-0.27	-0.47*	0.21	.38
Temporal	0.41*	-0.23	-0.39	0.16	.35
Occipital	0.27	-0.08	-0.19	0.01	.22
Thalamus	0.35	-0.34	-0.48*	0.17	.34
Basal forebrain Ch1-3	0.19	-0.11	-0.28	0.03	.36
Basal forebrain Ch4	0.15	-0.22	-0.24	0.16	.22

Note. PVE, partial volume effect; ROI, region of interest; Aβ, amyloid beta; MMSE, Mini Mental State Examination; AQ-D, discrepancy scores reflecting awareness of cognitive and behavioral functioning; MARS-FS, discrepancy scores reflecting awareness of memory functioning, DMS48, visual recognition memory. * $p < .05$; ** $p < .01$; *** $p < .005$ (Bonferroni correction for multiple tests).